UNIVERSITAT
JAUME·I

Título artículo / Títol article:

High-pressure synthesis, structural and complex magnetic properties of the ordered double perovskite Pb 2 NiReO 6

Autores / Autors

Teodora Stoyanova-Lyubenova , Antonio J. Dos santos-García, Esteban Urones-Garrote, María José Torralvo, Miguel Á. Alario-Franco

Revista:

Dalton Transactions

Versión / Versió:

Post-print

Cita bibliográfica / Cita bibliogràfica (ISO 690):

STOYANOVA-LYUBENOVA, Teodora, et al. High-pressure synthesis, structural and complex magnetic properties of the ordered double perovskite Pb 2 NiReO 6. *Dalton Transactions*, 2014, vol. 43, no 3, p. 1117-1124.

url Repositori UJI:

http://hdl.handle.net/10234/89398

High-Pressure synthesis, structural and complex magnetic properties of the ordered double perovskite Pb$_2$NiReO$_6$

Teodora Stoyanova-Lyubenova,[a] Antonio J. Dos santos-García,[*,a,b] Esteban Urones-Garrote,[c] María José Torralvo [a] and Miguel Á. Alario-Franco[*,a]

The ordered double perovskite Pb$_2$NiReO$_6$ has been prepared at 6 GPa and temperatures ranging from 1273-1373 K. Its crystal structure determined by X-ray powder diffraction and Selected Area Electron Diffraction shows monoclinic symmetry with centrosymmetric space group $I2/m$ (a=5.6021(1) Å, b= 5.6235(1) Å, c= 7.9286(1) Å and β= 90.284°(1)). High Angle Annular Dark Field microscopy studies reveal the existence of compositional microdomains. The compound displays a re-entrant spin-glass transition from a ferrimagnetic ordering below T$_N$ ~ 37 K between the Re^{+5} and Ni^{+3} (high spin configuration) magnetic sublattices to a spin-glass configuration. Magnetic field dependent magnetization measurements revealed wasp-waisted hysteresis loops at 5 K. These shaped features are originated from the antiferromagnetic/ferromagnetic (AFM/FM) competing interactions.

1 Introduction

Re-based double perovskites (A$_2$BB$'$O$_6$) where B$'$ site is occupied by Re ions are some of the most promising ferromagnetic oxides in terms of high Curie temperatures (T$_C$) since their discovery in the 60's of the last century[1]. For instance, Ca$_2$FeReO$_6$ (T$_C$ = 540 K), Sr$_2$FeReO$_6$ (T$_C$ = 400 K) or Sr$_2$CrReO$_6$ (T$_C$ = 635 K) highlight not only with large T$_C$, but also with high saturation magnetization and excellent magnetoresistance near room temperature[2–5]. The high magnetic ordering temperature in Re-based double perovskites can be attributed to the presence of one extra unpaired electron of Re^{+5} (5d^2: t$_{2g}^2$, S=1) cation compared to their Mo^{+5} analogues (4d^1: t$_{2g}^1$, S=1/2)[6–9]. Besides, the gradual decreasing of the A-cation radii reduces the symmetry from cubic $Fm\bar{3}m$ (Ba$_2$FeReO$_6$ T$_C$ = 303 K) through tetragonal $I4/m$ (Sr$_2$FeReO$_6$ T$_C$ = 400 K) to monoclinic $P2_1/n$ (Ca$_2$FeReO$_6$, T$_C$ = 522 K). Concomitantly to this, there also exist a reduction of the 180° B-O-Re angle which is mainly attributed to octahedral tilting[10]. The cubic (S. G. $Fm\bar{3}m$) compounds are metallic or their resistivity show little changes with temperature; but the tetragonal (S. G. $I4/m$) and monoclinic (S. G. $P2_1/n$) compounds present semiconducting and an insulating behavior respectively[11,12]. In addition, if a stereochemical active 6s^2 lone pair cation, such as Pb^{+2} is located at the A-position, it often induces strong anisotropy of the environment[13,14] that may create a polarization giving rise to dielectric, ferroelectric or piezoelectric properties[15–17]. Also, the insertion of Pb^{+2} at the A-site of the Sr$_2$FeReO$_6$ semiconducting perovskite will lead to an expected decrease of the

B-O-Re angle which will make Pb$_2$NiReO$_6$ become insulator[18,19]. It was published elsewhere the synthesis of a complete series of Pb$_2$MReO$_6$ perovskites (M= Ni^{+3}, Fe^{+3}, Mn^{+3}, etc.)[20–22]. It was reported that these compounds crystallize in the $Fm\bar{3}m$ cubic space group with parameter 2a$_p$ (where a$_p$ ~ 4 Å is the lattice constant of the ABO$_3$ cubic perovskite). Concerning the magnetic properties of these compounds, it was assumed that several members of the Pb$_2$MReO$_6$ series (M = Fe and Ni) were ferrimagnetic, while Pb$_2$CoReO$_6$ shows antiferromagnetic properties[21]. However neither further details on their crystal structure nor magnetic characterization were performed at that time. Recently, it was confirmed the ferrimagnetic behavior of Pb$_2$FeReO$_6$ (T$_C$ = 420 K) which seems also to be a semiconductor[23]. The Pb$_2$FeReO$_6$ perovskite is centrosymmetric (S. G. $I4/m$) but no structural transition was observed at low temperatures. Another member of the Pb$_2$MReO$_6$ series, e.g. Pb$_2$MnReO$_6$, was also studied[24]. This double perovskite crystallized with monoclinic symmetry (S. G. $P2_1/n$) and shows a T$_C$ ~ 100 K and semiconducting properties. To the best of our knowledge, there does not seem to be further studies concerning some other Pb$_2$MReO$_6$ members. Taking into account these considerations, we have revisited the structure, microstructure and magnetic properties of the Pb$_2$NiReO$_6$ member[20]. In light of our results we have been able to determine the crystal structure and a complex microstructure. We have also established a much more elaborated magnetic behavior which operates on the lead nickel

rhenate Pb_2NiReO_6 perovskite.

2 Experimental Section

2.1 Sample preparation

It had been previously reported that the room pressure synthesis of Pb_2MReO_6 compositions leads to the formation of oxygen deficient pyrochlores[24,25]. Therefore, the materials have been prepared by solid state reaction at high-pressure and high-temperature using a Belt-type press located at the "High Pressure Laboratory" from Complutense University (Madrid, Spain). Powdered samples of Pb_2NiReO_6 were obtained, starting from stoichiometric amounts of PbO (Sigma-Aldrich, 99%), NiO (Sigma-Aldrich, 99%) and ReO_3 (Sigma-Aldrich, 99%). The precursor oxides were grounded together in an agate mortar under acetone and further dried at air. The solid state reaction took place into a 12 mm platinum pressure cell, at 1273 K and 1373 K for 60 min under 6 GPa of pressure using a heating rate of 25 W/min and 300 tons/h of pressure increase rate. Afterwards, the temperature was quenched and the pressure was slowly released until room pressure values. It is important to mention here that we are dealing with high pressure synthesis and, usually, samples contain a certain amount of secondary phases. In this connection, although the samples are nearly single phases, a few weak extra reflections from $Pb(ReO_4)_2$, $Ni(ReO_4)_2$ and PbO_2 are seen in the Pb_2NiReO_6 1273 K XRD pattern (Figure 1a). The high pressure modification of the ReO_3 perovskite, $PbRe_2O_6$ and also the $Pb(ReO_4)_2$ are the phases apparent in the case of Pb_2NiReO_6 1373 K as seen in the XRD pattern (Figure 1b). In what follows, the samples will be referred in the text as: Pb_2NiReO_6-LT prepared at 1273 K and Pb_2NiReO_6-HT obtained at 1373 K.

2.2 Structure and Microstructure analysis

X-ray powder diffraction data were collected on a Phillips XPert PRO ALPHA 1 diffractometer with Cu-Kα_1 radiation, equipped with a Ge (111) monochromator, working on the BraggBentano geometry. X-ray diffraction data were obtained in the range of $10° < 2\Theta < 120°$ with a step size of $0.017°$ collected for 150 s. Rietveld refinements of these data were performed using the FullProf software package[26]. Background was fitted using a linear interpolation and peak shapes were modelled according to a Thompson-Cox-Hastings function. For transmission electron microscopy (TEM), the samples were grinded in n-butyl alcohol and ultrasonically dis-

[a] Dpto. de Química Inorgánica, Facultad de Químicas, Universidad Complutense de Madrid, 28040 Spain. E-mail: maaf@ucm.es
[b] Dpto. de Química Industrial y Polímeros, E.U.I.T.I, Universidad Politecnica de Madrid, 28012 Spain. E-mail: aj2santosgarcia@gmail.com
[c] Centro Nacional de Microscopía electronica, Universidad Complutense de Madrid, 28040 Spain.

persed. A few drops of the resulting suspension were deposited on holey carbon-coated copper grids. Selected area electron diffraction (SAED) studies were performed in an electron microscope JEOL 2000FX with double tilt (45°) working at 200 kV. The composition was checked in situ with an Oxford Link ISIS 300 microanalysis system (X-Ray energy dispersive spectroscopy - EDS) coupled to the microscope. The metal-atomic ratio quantified on approximately 30 crystallites, showed that Pb, Ni and Re are in the proportion that we intended and, therefore, in agreement with the expected stoichiometric composition. High Resolution Transmission Electron (HRTEM) studies and High Angle Annular Dark Field (HAADF) scanning transmission electron microscopy (STEM) were carried out with a JEM 3000F microscope operating at 300 kV (double tilt of 20° and point resolution 1.7 Å), fitted with an ENFINA 1000 spectrometer and a JEOL annular dark field (ADF) detector. The HAADF-STEM images were acquired with a collection angle of ~ 30 mrad, and their contrast is directly related to the atomic number of the present atoms (Z-contrast imaging).

2.3 Magnetic measurements

Magnetic susceptibility measurements were performed over the temperature range 2 -300 K, using a Squid Quantum Design XL-MPMS magnetometer under DC zero-field-cooling (ZFC) and field-cooling (FC) conditions, using a DC magnetic field of 1000 Oe. Furthermore, AC Susceptibility data was recorded at 1, 100 and 1000 Hz frequencies with an AC field of 3.5 Oe in amplitude. Magnetization Hysteresis loops were collected at 5 K and magnetization measurements as a function of the applied magnetic field (H) were performed at 100 K.

3 Results and Discussion

3.1 Structural and microstructural characterization

The powder XRD diagrams (Figure 1a, b) at room temperature are characteristic of a perovskite type structure. Initial attempts to fit the XRD patterns of both samples were made in the tetragonal $I4/m$ space group since other rhenium-containing double perovskites, for instance Pb_2MReO_6 and Sr_2MReO_6, also crystallize in this space group[23,27]. Although these initial fittings (data not shown) seemed acceptable, a careful examination of the patterns showed the occurrence of some subtle splitting of the main reflections. In this connection, Figures 2a and 2b show the orthorhombic/monoclinic distortion that splits the 200 and 112 tetragonal reflections (Figure 2a) to the combination of the 200/020 and 112/-112 maxima respectively (Figure 2b). This distortion is also accompanied by the appearance of some weak superlattice peak-
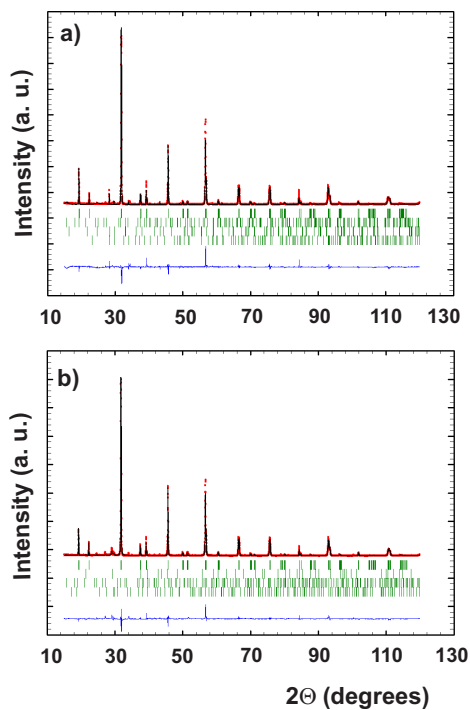
Fig. 1 (Rietveld refinement of the XRD powder patterns of (a) Pb_2NiReO_6-LT and (b) Pb_2NiReO_6-HT samples. Red points, upper and lower solid line show observed, calculated and difference patterns respectively. Sticks correspond to Pb_2NiReO_6 (1st row), $Pb(ReO_4)_2$ (2nd row), $Ni(ReO_4)_2$ (3rd row) and PbO_2 (4th row) for sample Pb_2NiReO_6-LT. Sticks correspond to Pb_2NiReO_6 (1st row), ReO_3 (2nd row), $Pb(ReO_4)_2$ (3rd row) and $PbRe_2O_6$ (4th row) for sample Pb_2NiReO_6-HT.
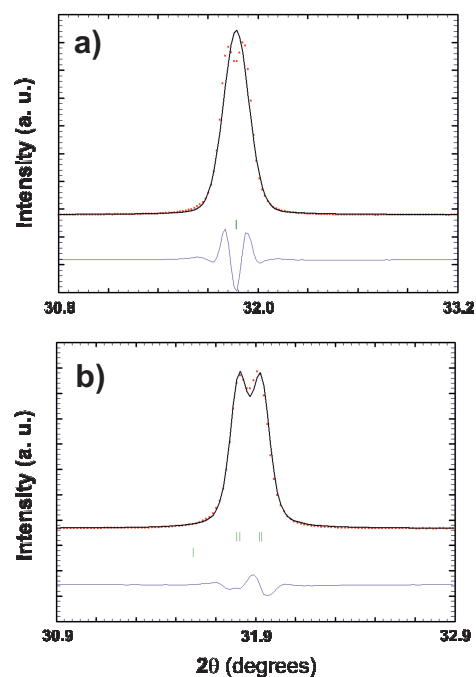

Fig. 2 Observed (points), calculated (full line), and differences (bottom line) profiles of the Rietveld refinement of the XRD patterns corresponding to the fit (a)using the tetragonal $I4/m$ and (b) the monoclinic $I2/m$ space groups. See in the text for more clarifications.
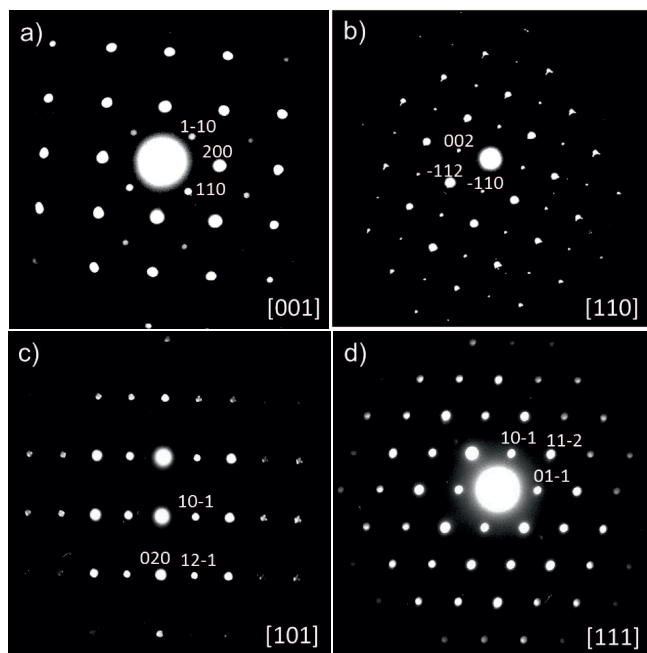
Fig. 3 SAED patterns along the (a) [001], (b) [110], (c) [101], and (d) [111] directions for the Pb_2NiReO_6-LT compound.

Fig. 4 Electron micro-diffraction pattern of Pb_2NiReO_6-LT along [101] zone axis.

s due to octahedra tilting in consecutive layers. However, it is worth noting that not all the superlattice reflections can be detected by XRD as they depend on weak anion scattering. Further Rietveld refinements were made using the monoclinic $P2_1/n$ and orthorhombic Pbnm space groups, since these are the most common space groups found in ordered and disordered perovskites respectively[28]. It is also important to stress that the peak positions could also be explained assuming the monoclinic $I2/m$ space group, which is in fact a subgroup of tetragonal $I4/m$, allowing 1:1 cation ordering at the B-site of the perovskite structure. These three structures are closely related and, although they exhibit different octahedral tilt systems, that is, a 3-tilt system ($a^+b^-b^-$) for both Pbnm and $P2_1/n$ and 2-tilt system ($a^0b^-c^-$) for $I2/m$[29], it is difficult to distinguish an orthorhombic random sublattice from a monoclinic rock salt sublattice when the monoclinic angle is near $90°$. Taking into account the poor X-Ray scattering from the oxygen atoms concomitantly to the presence of some other heavy ones, i. e. Pb, Ni and Re, all these models gave reasonable fittings for the splitting of these reflections. In order to clarify these structural uncertainties, SAED patterns along the main crystallographic zones were collected (Figure 3a-d).

The observed Bragg reflections correspond to a perovskite cell with size $\sqrt{2}a_p$ x $\sqrt{2}a_p$ x $2a_p$ (this is the so-called diagonal perovskite superstructure). These results did not discard the possibility of an orthorhombic or monoclinic cell, so that $P2_1/n$, Pbnm and $I2/m$ space groups were still considered. At
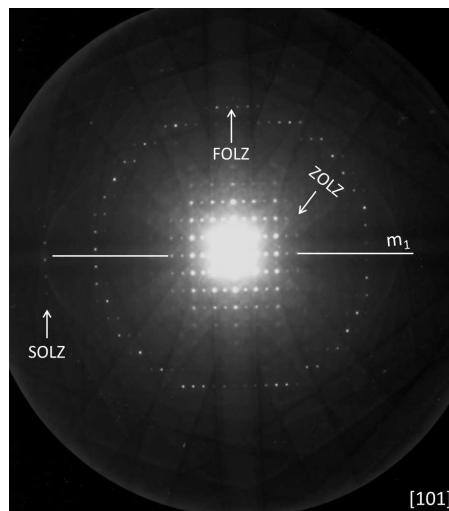
this point, in order to shed light into the space group of these compounds, we have studied the symmetry by means of Zone Axis Microdiffraction Patterns (ZAP). It is well known that, microdiffraction patterns obtained with a covergent electron beam allows one to obtain direct information about the crystal system and the Bravais lattice and to reveal the presence of glide planes and screw axes of a specimen[30]. Therefore, one can distinguish the Bravais lattice, between $I2/m$ and Pbnm (or $P2_1/n$) space groups, taking into account the relative positions of the reflections in high-order Laue zones (HOLZ) compared to those in the zero-order Laue zone (ZOLZ). As shown in Figure 4, the [101] zone axis microdiffraction pattern shifts between the nets of reflections situated in the ZOLZ and in the FOLZ are observed. As a result, this periodicity difference is consistent with an I-centered lattice; therefore, we are in the position to unambiguously establish that $I2/m$ is the correct space group for these Pb_2NiReO_6 perovskites. Moreover, the mesh of reflections of the FOLZ (m symmetry) and the ZOLZ (2mm symmetry) are characteristics for 2/m point group and fit with $I2/m$ space group determination[30]. Taking this result into account, the Rietveld refinement of the X-ray diffraction data, shown in Figures 1a and 1b, were performed using the monoclinic $I2/m$ space group. The structure parameters, crystallographic data, selected bond distances and angles, and agreement factors are listed in Table I and II.

It is interesting to mention that, in both refinements; we have considered a degree of mixing between Ni and Re sites. There is no evidence of cation disordering in the Pb_2NiReO_6-LT sample and, only a 5.2% of Re cations were found at the Ni positions and vice versa in the Pb_2NiReO_6-HT one. This is indeed a clear indication that the octahedral-site cations are

Table 1 Atomic positions, selected angles and distances, and agreement factors for Pb_2NiReO_6-LT obtained from Rietveld refinement of the XRD data[a].

[a] a = 5.6021 (1) Å, b = 5.6238 (1) Å, c = 7.9287 (1) Å, β = 90.284°(1), V = 249.795 (8)Å³, R_p = 15.4, R_B = 9.37, R_f = 8.14 χ^2 = 7.57

atom	site	x/a	y/b	z/c	Occ
Pb	4i	0.4973(6)	0	0.2543(4)	0.467(2)
Ni	2a	0	0	0	0.25
Re	2d	0	0.5	0	0.25
O1	4i	0.016(9)	0	0.266(6)	0.5
O2	8j	0.226(5)	0.292(4)	0.009(4)	1

(Ni-O_1)= 2.11 (4)× 2	(Re-O_1)= 1.86 (5)× 2
(Ni-O_2)= 2.07(2)× 4	Re-O_2)= 1.93 (2)× 4
∠(Ni-O_1-Re) = 174.8 (2)	∠(Ni-O_2-Re) = 164.4 (1)

Table 2 Atomic positions, selected angles and distances, and agreement factors for Pb_2NiReO_6-HT obtained from Rietveld refinement of the XRD data[a].

[a] a = 5.6027(1)Å, b = 5.6224(1) Å, c = 7.9311(1) Å, β = 90.269°(1), V = 249.832 (8)Å³, R_p = 10.5, R_B = 6.97, R_f = 6.93 χ^2 = 7.24

atom	site	x/a	y/b	z/c	Occ
Pb	4i	0.4949(4)	0	0.2555(3)	0.464(2)
Ni1	2a	0	0	0	0.236(1)
Re1	2a	0	0	0	0.014(1)
Ni2	2d	0	0.5	0	0.014(1)
Re2	2d	0	0.5	0	0.236(1)
O1	4i	0.043(7)	0	0.248(5)	0.5
O2	8j	0.215(4)	0.300(3)	-0.003(1)	1

(Ni-O_1)= 1.98 (4) × 2	(Re-O_1)= 2.01 (4)× 2
(Ni-O_2)= 2.06(2)× 4	Re-O_2)= 1.96 (2)× 4
∠(Ni-O_1-Re) = 175.0 (6)	∠(Ni-O_2-Re) = 161.1 (8)

ordered in a rock-salt configuration. It is also worth noting that both samples are Pb-deficient. The Pb-deficiency obtained by the Rietveld refinement is as less as 0.066 and 0.072 for the LT- and HT-samples respectively. The octahedral distortions where calculated from the formula

$$\Delta = \frac{1}{6}\sum_{i=1}^{6}\left(\frac{d_i - d_{av}}{d_{av}}\right)^2 \qquad (1)$$

where d_{av} is the average distance of the Ni-O and Re-O bonds, take the value of $\Delta Ni = 0.66 \times 10^{-4}$ and $\Delta Re = 3.31 \times 10^{-4}$ for the Pb_2NiReO_6-LT sample and, $\Delta Ni = 3.72 \times 10^{-4}$ and $\Delta Re = 1.7 \times 10^{-4}$ for the Pb_2NiReO_6-HT one. In light of these calculations one can clearly see that there is no Jahn-Teller effect, in agreement with Ni^{+3} (S = 3/2, that is, high spin configuration) and Re^{+5} (S = 1) electronic configurations. The small site-exchange positions produce a small alteration in the $[M-O_6]$ octahedra, owing to differences in the Ni^{+3} and Re^{+5} cation sizes. On the other hand, the Ni-O_1-Re bond angles running along the c-axis are 174.8° and 175° for Pb_2NiReO_6-LT and -HT samples respectively, while the Ni-O_2-Re ones, lying a-long the ab-plane, are reduced to 164.4° and 161.1° for the Pb_2NiReO_6-LT and -HT samples respectively. The magnitude of the tilt angle has been estimated from the refined atomic coordinates[31]. The tilt angle for $I2/m$ space group ($a^0b^-c^-$), having an out-of-phase tilt about the [110] axis, where calculated from the expression

$$\tan\phi = \frac{1}{3}\left(\frac{4x_1 a}{c} - \frac{8z_2 c}{a}\right) \qquad (2)$$

where z_2 and x_1 refer to the atomic coordinates for O(1) and O(2) in Table 1, respectively. The magnitudes of these octahedral tilting angles are less than 3° for both samples, -1.1° and 2.9° LT and HT respectively. All these structural considerations are in concordance with the observed magnetic properties of both samples (see below).

3.2 Magnetic properties

The temperature dependence of the magnetic susceptibility for Pb_2NiReO_6-LT, measured from 300 down to 2 K at ZFC and FC modes at 1000 Oe are depicted in Figure 5. The experimental magnetic moment calculated from the linear interpolation of the corresponding reciprocal susceptibility plot performed at temperatures well above within the paramagnetic regime, i. e. 300-200 K, takes the value of 4.31 μB. This value agrees rather well with the calculated (4.79 μB), corresponding to Re^{+5} (S = 1) and Ni^{+3} (S = 3/2, that is, high spin configuration) paramagnetic cations. Taking into account the negative Weiss temperature, -222.85 K, it is reasonable to expect frustrated antiferromagnetic (AFM) interactions. On cooling below 50 K, the ZFC susceptibility deviates increasingly form the Curie-Weiss behavior, with a sharp maximum centred
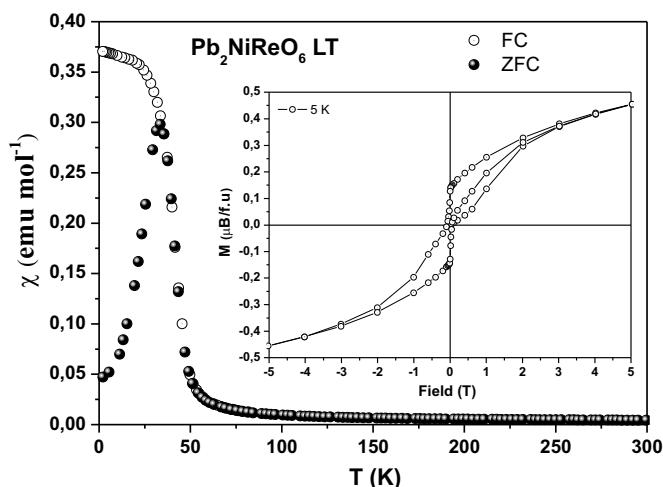
Fig. 5 Temperature dependence of magnetic susceptibility of Pb_2NiReO_6-LT under external field of 1000 Oe. Magnetization curve (M vs. H) at 5 K (inset).
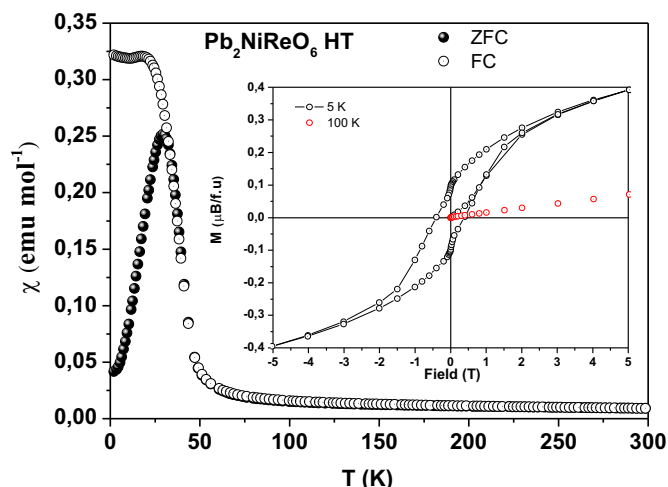

Fig. 6 Temperature dependence of magnetic susceptibility of Pb_2NiReO_6-HT under external field of 1000 Oe. Magnetization curve (M vs. H) at 5 and 100 K (inset).

around 37 K which, at a first sight, can be attributed to the presence of antiferromagnetic interactions. However, there also exists, below this temperature, a notable divergence between the ZFC and FC plots which, in general terms, is indicative of the existence of a net ferromagnetic component. It is also important to stress that, this strong difference has normally been observed in magnetic systems frozen in a spin-glass configuration[32]. Magnetic hysteresis measurements (inset of Figure 5) indicate a non-linear M-H variation at 5 K, characterized by a wasp-waisted shape loop. The magnetic moment at this temperature and at a magnetic field of 5 T, takes the value of 0.45 μB, far from the theoretical saturation value of 5 μB, assuming a ferromagnetic coupling between the Re^{+5} (S = 1) and Ni^{+3} (S = 3/2) magnetic sublattices. This suggests that the ferromagnetic component arises from a ferrimagnetic ordering between both magnetic sublattices.

On the other hand, Figure 6 shows the corresponding temperature dependence magnetic susceptibility for Pb_2NiReO_6-HT sample. At temperatures well above T_N, the compound behaves as a paramagnet (see 100 K plot at inset of Figure 6) and, a similar deviation from the Curie-Weiss behavior is also observed in this sample below 50 K. However, clear differences are apparent in the field dependent magnetization measurements below this transition; below T_N, a soft wasp-waisted hysteresis loop is observed. It is also interesting to note, that the saturation moment value (0.39 μB) is close to that observed for the Pb_2NiReO_6-LT sample. The origin of the striking feature observed in the wasp-waisted hysteresis loops results from a mixture of magnetic components with contrasting coercivities[33], i. e. FM and AFM components. Such a mixture will result in a bias of the magnetic parame-
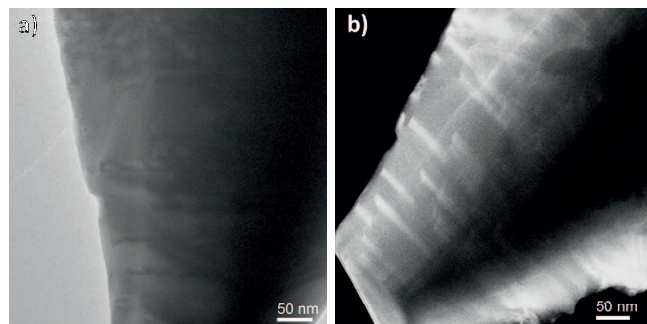

Fig. 7 a) Low-magnification TEM image of the Pb_2NiReO_6-LT sample. b) HAADF-STEM image of the same crystal.

ters towards one or another constituent, producing distinctive wasp-waisted shapes; the degree of wasp-waistedness will be dependent on the relative contribution of each component[33]. In order to shed light into this shaped features, a detailed microstructural characterization was performed. An initial TEM study revealed some contrast irregularities in the micrograph corresponding to the Pb_2NiReO_6-LT, as can be clearly seen in Figure 7a. Further complementary studies using high-angle annular dark field (HAADF) images showed a clear situation in that, bright zones are intercalated into a dark matrix (Figure 7b). It is important to recall that, the HAADF technique is extremely sensible to the variation in the atomic number and allows one to establish compositional variations in the materials. In fact, bright zones will indeed correspond to Re-rich compositional domains within the matrix. On the other hand, a more homogeneous contrast without bright and dark areas is observed on the HAADF micrograph, depicted in Figure 8,
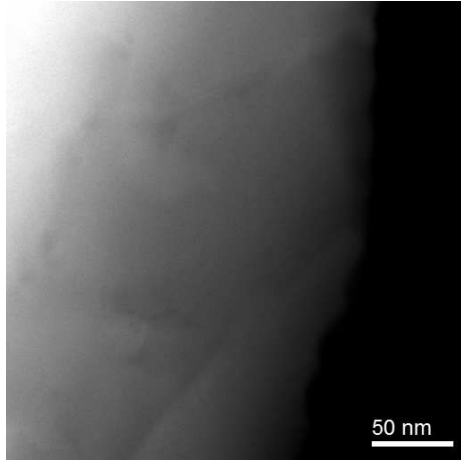
Fig. 8 HAADF-STEM image of a crystal belonging to the Pb$_2$NiReO$_6$-HT sample.

of the Pb$_2$NiReO$_6$-HT sample, which confirms the absence in this case of compositional domains.

In Pb$_2$NiReO$_6$, the Ni and Re ions are paramagnetic and therefore, its magnetic properties must arise from the combination of Re^{+5} and Ni^{+3} magnetic sublattices. As described in the structural analysis, Pb$_2$NiReO$_6$ is an ordered double perovskite where both Ni and Re atoms are arranged in alternating corner-sharing octhaedra. Therefore Ni^{+3}-O-Re^{+5} superexchange interactions will govern the overall magnetic interactions apparent in these compounds. Taking into account the Ni-O$_1$-Re and Ni-O$_2$-Re angles and the electronic configurations of the paramagnetic cations, the nature of the magnetic interactions is expected to be moderately ferromagnetic[34]. On the other hand, the sign of the magnetic interactions of the Re-rich domains will be governed by weak AFM interactions resulting from the Re-O-Re superexchange pathways. Therefore, two mechanisms compete one against another giving rise to these uncommon wasp-waisted features. It is also important to stress that, the mixed FM- AFM interactions install the competition and ensure co-operativeness of a freezing process[35,36]. In fact, the huge negative value of the Weiss constant (Θ = -222.85 K) is indeed a clear indication of the presence of magnetic frustration that is a direct consequence of the disordered and mixed interactions[32]. It is interesting to note that magnetic frustration has been previously observed in some other compounds containing 3d-5d superexchange interactions[37]. In order to shed light into this configuration we have also performed temperature dependence susceptibility measurements in AC mode for both samples. From one hand, Figure 9a and 10a show the dispersion in the real part of the χ' vs. T plots at frequencies running from 1 to 1000 Hz with an amplitude of 3 Oe; on the other hand Figure 9b and 10b show the absorption in the imaginary part χ''
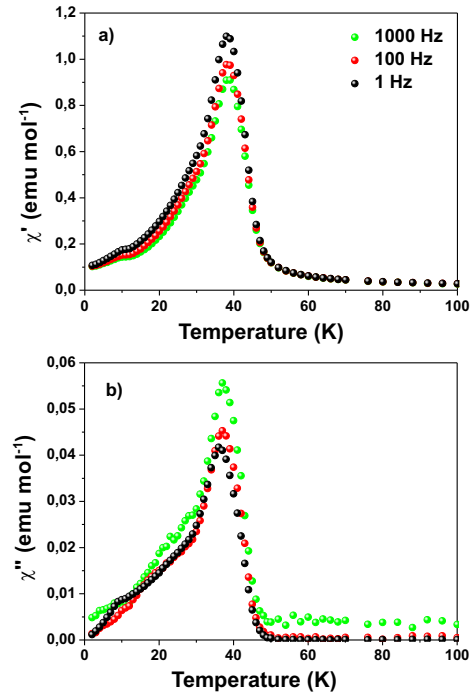

Fig. 9 a) Real χ' and b) imaginary χ'' part of the ac-susceptibility for the Pb$_2$NiReO$_6$-LT sample.

vs. T plots for the Pb$_2$NiReO$_6$-LT and Pb$_2$NiReO$_6$-HT respectively. The real part of the ac susceptibility shows the existence of sharp (Figure 9a) and rather rounded peaks (Figure 10a) at 37 K which have no frequency dependence. It is interesting to note that shoulders at 10 K and 30 K do also appear in the χ' (T) curve for the LT and HT samples respectively and are strongly dependent of the frequency within the probed range indicating the presence of glassy nature at lower temperatures. These changes are more noticeable in the corresponding out-of-phase components (χ''), depicted in Figures 9b and 10b. These findings evince a re-entrant spin-glass transition (RSG) from a ferrimagnetic long-range-ordering at T$_N$ 37 K to spin-glass with freezing temperatures T$_f$ 10 K and 30 K for Pb$_2$NiReO$_6$-LT and Pb$_2$NiReO$_6$-HT compounds respectively. The differences observed in the freezing temperatures between both samples are clearly indicative of the different size and shape of the Re-rich AFM domains as it has been previously observed in the HAADF micrographs. The size and shape of these domains also govern the wasp-waistedness of the hysteresis.

4 Conclusions

Pb$_2$NiReO$_6$ double perovskites were prepared by high pressure and high temperature synthesis method. The crystal structure is defined in a monoclinic unit cell (space group
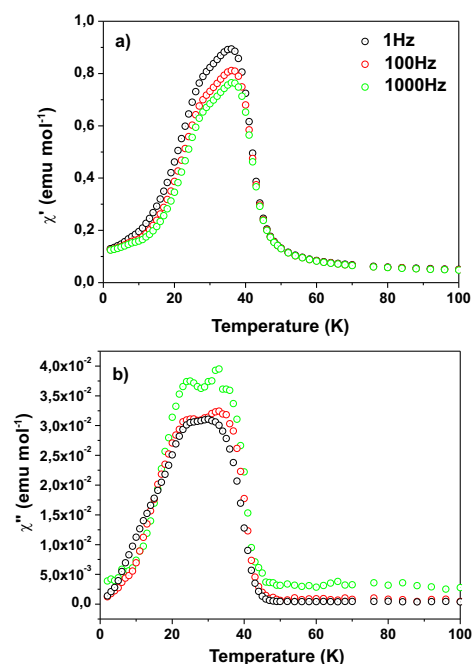
Fig. 10 a) Real χ' and b) imaginary χ'' part of the ac-susceptibility for the Pb_2NiReO_6-HT sample.

$I2/m$); the crystal contains alternating $[NiO_6]$ and $[ReO_6]$ octahedra tilted in antiphase along the b and c axis ($a^0b^-c^-$). The compounds display a RSG-transition from ferrimagnetic ordering ($T_N \sim 37$ K), which arise from the coupling of Re^{+5} and Ni^{+3} (high spin configuration) magnetic sublattices, to a spin-glass configuration at low temperatures. Magnetic field dependent magnetization measurements show a very interesting behavior characterized by wasp-waisted hysteresis loops at 5 K. These shaped features are originated from the AFM/FM competing interactions occurring in compositional microdomains found in these samples. The mixed FM-AFM interactions install the competition and ensure co-operativeness of the observed freezing process at low temperatures.

5 Acknowledgements

References

1 A. W. Sleight, J. Longo and R. Ward, *Inorganic Chemistry*, 1962, **1**, 245–250.

2 J. D. Teresa, D. Serrate, J. Blasco, M. Ibarra and L. Morellon, *Journal of Magnetism and Magnetic Materials*, 2005, **290-291, Part 2**, 1043 – 1049.

3 D. Serrate, J. M. D. Teresa and M. R. Ibarra, *Journal of Physics: Condensed Matter*, 2007, **19**, 023201.

4 F. D. Czeschka, S. Geprags, M. Opel, S. T. B. Goennenwein and R. Gross, *Applied Physics Letters*, 2009, **95**, 062508.

5 M. Retuerto, M. Martnez-Lope, M. Garca-Hernndez and J. Alonso, *Materials Research Bulletin*, 2009, **44**, 1261 – 1264.

6 D. D. Sarma, P. Mahadevan, T. Saha-Dasgupta, S. Ray and A. Kumar, *Phys. Rev. Lett.*, 2000, **85**, 2549–2552.

7 A. Arulraj, K. Ramesha, J. Gopalakrishnan and C. Rao, *Journal of Solid State Chemistry*, 2000, **155**, 233 – 237.

8 T.-T. Fang, M. Wu and T. Ko, *Journal of Materials Science Letters*, 2001, **20**, 1609–1610.

9 M. J. Martinez-Lope, J. A. Alonso, M. T. Casais and M. T. Fernandez-Diaz, *European Journal of Inorganic Chemistry*, 2002, **2002**, 2463–2469.

10 J. M. De Teresa, D. Serrate, J. Blasco, M. R. Ibarra and L. Morellon, *Phys. Rev. B*, 2004, **69**, 144401.

11 A. Winkler, N. Narayanan, D. Mikhailova, K. G. Bramnik, H. Ehrenberg, H. Fuess, G. Vaitheeswaran, V. Kanchana, F. Wilhelm, A. Rogalev, A. Kolchinskaya and L. Alff, *New Journal of Physics*, 2009, **11**, 073047.

12 J. Gopalakrishnan, A. Chattopadhyay, S. B. Ogale, T. Venkatesan, R. L. Greene, A. J. Millis, K. Ramesha, B. Hannoyer and G. Marest, *Phys. Rev. B*, 2000, **62**, 9538–9542.

13 A. M. Arevalo-Lopez and M. A. Alario-Franco, *Journal of Solid State Chemistry*, 2007, **180**, 3271–3279.

14 A. M. Arevalo-Lopez, A. J. Dos Santos-Garcia and M. A. Alario-Franco, *Inorganic Chemistry*, 2009, **48**, 5434–5438.

15 N. A. Hill, *The Journal of Physical Chemistry B*, 2000, **104**, 6694–6709.

16 TOMASHPO.YY, VENEVTSE.YN and G. ANTONOV, *SOVIET PHYSICS JETP-USSR*, 1966, **22**, 255–&.

17 S. A. Larregola, J. A. Alonso, J. C. Pedregosa, M. J. Martinez-Lope, M. Alguero, V. De la Pena-O'shea, F. Porcher and F. Illas, *Dalton Trans.*, 2009, **0**, 5453–5459.

18 H. Iwasawa, T. Saitoh, Y. Yamashita, D. Ishii, H. Kato, N. Hamada, Y. Tokura and D. D. Sarma, *Phys. Rev. B*, 2005, **71**, 075106.

19 K. Oikawa, T. Kamiyama, H. Kato and Y. Tokura, *Journal of the Physical Society of Japan*, 2003, **72**, 1411–1417.

20 V. V. Gagulin, N. V. Fadeeva, A. G. Belous, L. A. Sevastianova, A. V. Titov, M. V. Plotnikova, K. P. Mitrofanov, E. V. Zubova, S. P. Solovev and Y. N. Venevtsev, *physica status solidi (a)*, 1977, **44**, 247–257.

21 Y. VENEVTSEV, S. SOLOVIEV, V. GAGULIN, N. FADEEVA, A. BELOUS, A. TITOV, K. MITROFANOV, M. PLOTNIKOVA, L. SEVASTIANOVA and E. ZUBOVA, *FERROELECTRICS*, 1978, **21**, 411–412.

22 L. SEVASTYANOVA, E. ZUBOVA, V. GAGULIN and Y. VENEVTSEV, *ZHURNAL NEORGANICHESKOI KHIMII*, 1979, **24**, 3213–3217.

23 K. Nishimura, M. Azuma, S. Hirai, M. Takano and Y. Shimakawa, *Inorganic Chemistry*, 2009, **48**, 5962–5966.

24 K. Ramesha, L. Sebastian, B. Eichhorn and J. Gopalakrishnan, *Chemistry of Materials*, 2003, **15**, 668–674.

25 K. Ramesha, L. Sebastian, B. Eichhorn and J. Gopalakrishnan, *J. Mater. Chem.*, 2003, **13**, 2011–2014.

26 J. Rodrguez-Carvajal, *Physica B: Condensed Matter*, 1993, **192**, 55 – 69.

27 M. Retuerto, M. J. Martnez-Lope, M. Garca-Hernndez, M. T. Fernndez-Daz and J. A. Alonso, *European Journal of Inorganic Chemistry*, 2008, **2008**, 588–595.

28 M. T. Anderson, K. B. Greenwood, G. A. Taylor and K. R. Poeppelmeier, *Progress in Solid State Chemistry*, 1993, **22**, 197 – 233.

29 A. M. Glazer, *Acta Crystallographica Section B*, 1972, **28**, 3384–3392.

30 J. Morniroli and J. Steeds, *Ultramicroscopy*, 1992, **45**, 219 – 239.

31 K. S. Wallwork, B. J. Kennedy, Q. Zhou, Y. Lee and T. Vogt, *Journal of Solid State Chemistry*, 2005, **178**, 207 – 211.

32 J. A. Mydosh, *Spin glasses : an experimental introduction*, Taylor and Francis London ; Washington, DC, 1993.

33 L. H. Bennett and E. D. Torre, *Journal of Applied Physics*, 2005, **97**, 10E502.

34 J. B. Goodenough, *Magnetism and the Chemical Bond*, Interscience (Wiley), New York, 1963.

35 M. Viswanathan and P. S. A. Kumar, *Phys. Rev. B*, 2009, **80**, 012410.

36 A. J. Dos Santos-Garcia, J. V. Duijn and M. A. Alario-Franco, *Journal of Solid State Chemistry*, 2008, **181**, 3317 – 3321.

37 P. Battle, S. Bollen and A. Powell, *Journal of Solid State Chemistry*, 1992, **99**, 267 – 275.